





Article

Beyond Chelation: EDTA Tightly Binds Taq DNA Polymerase, MutT and dUTPase and Directly Inhibits dNTPase Activity

Anna Lopata ^{1,2,3}, Balázs Jójárt ⁴ , Éva V. Surányi ^{1,2} , Enikő Takács ¹, László Bezúr ⁵,
Ibolya Leveles ^{1,2}, Ábris Á. Bendes ^{1,6} , Béla Viskolcz ⁷ , Beáta G. Vértessy ^{1,2} and Judit Tóth ^{1,*}

¹ Institute of Enzymology, Research Centre for Natural Sciences, Hungarian Academy of Sciences, 1113 Budapest, Hungary; lopata.anna@gmail.com (A.L.); suranyi.eva@ttk.mta.hu (É.V.S.); enikot@gmail.com (E.T.); leveles.ibolya@ttk.mta.hu (I.L.); abris.bendes@oulu.fi (Á.Á.B.); vertessy@kutatok.org (B.G.V.)

² Department of Applied Biotechnology, Budapest University of Technology and Economics, 1111 Budapest, Hungary

³ Institute of Biophysical Chemistry, Goethe University, 60438 Frankfurt am Main, Germany

⁴ Institute of Food Engineering, Faculty of Engineering, University of Szeged, 6724 Szeged, Hungary; jojartb@gmail.com

⁵ Department of Inorganic and Analytical Chemistry, Budapest University of Technology and Economics, 1111 Budapest, Hungary; bezur@mail.bme.hu

⁶ Faculty of Biochemistry and Molecular Medicine, University of Oulu, 90220 Oulu, Finland

⁷ Institute of Chemistry, University of Miskolc, 3515 Miskolc, Hungary; bela.viskolcz@uni-miskolc.hu

* Correspondence: toth.judit@ttk.mta.hu; Tel.: +36-1382-67-93

Received: 11 September 2019; Accepted: 15 October 2019; Published: 17 October 2019



Abstract: EDTA is commonly used as an efficient chelator of metal ion enzyme cofactors. It is highly soluble, optically inactive and does not interfere with most chemicals used in standard buffers making EDTA a common choice to generate metal-free conditions for biochemical and biophysical investigations. However, the controversy in the literature on metal-free enzyme activities achieved using EDTA or by other means called our attention to a putative effect of EDTA beyond chelation. Here, we show that EDTA competes for the nucleotide binding site of the nucleotide hydrolase dUTPase by developing an interaction network within the active site similar to that of the substrate. To achieve these findings, we applied kinetics and molecular docking techniques using two different dUTPases. Furthermore, we directly measured the binding of EDTA to dUTPases and to two other dNTPases, the Taq polymerase and MutT using isothermal titration calorimetry. EDTA binding proved to be exothermic and mainly enthalpy driven with a submicromolar dissociation constant considerably lower than that of the enzyme:substrate or the Mg:EDTA complexes. Control proteins, including an ATPase, did not interact with EDTA. Our findings indicate that EDTA may act as a selective inhibitor against dNTP hydrolyzing enzymes and urge the rethinking of the utilization of EDTA in enzymatic experiments.

Keywords: dNTP hydrolysis; EDTA; dNTP pool sanitizing enzymes; dNTPase inhibitor

1. Introduction

Divalent metal ions including Mg^{2+} , Cu^{2+} , Fe^{2+} , Mn^{2+} , Ni^{2+} , and Zn^{2+} play prominent roles in enzymatic catalysis. The small organic compound ethylene diamine tetraacetic acid or commonly known as EDTA is frequently used to chelate these metal ions to investigate enzyme function in the absence of metal co-factors. This molecule comprises four carboxylic acid groups, thus have an

overall negative charge. Its structure is flexible when unbound and adopts a rigid conformation while complexed with a single divalent metal ion (Me^{2+}). All four carboxylic acid groups and two amines are involved in the hexacoordinated EDTA: Me^{2+} complex. It is highly soluble, optically inactive, and does not interfere with most chemicals used in standard buffers. Thus, EDTA seems to be a beneficial and safe choice to generate metal-free conditions for biochemical and biophysical investigations.

For enzymes catalyzing the hydrolysis of nucleotides to yield (d)NDP and P_i (inorganic phosphate) (e.g., ATPases [1], GTPases [2]) or (d)NMP + PP_i (e.g., ligases [3], DNA and RNA polymerases [4], Nudix hydrolases [5], and dUTPases) metal ions, notably Mg^{2+} , are usually considered to be of high functional importance. In most cases, k_{cat} (steady-state catalytic activity) values are reported to decrease by several orders of magnitude in lack of these metal ions. Nucleotide hydrolyzing enzymes can operate with either one or two Mg^{2+} ions bound. The enzyme dUTPase is a preventive DNA repair protein that hydrolyses dUTP into dUMP and pyrophosphate, performing a dNTP pool sanitizing role. Thereby it prevents uracil incorporation into DNA that would eventually lead to hyperactive DNA repair cycles and cell death [6]. In most species, it forms a homotrimer with three active sites that are built up from five conserved motifs [6]. The substrate dUTP- Mg^{2+} complex binds to the active site and is coordinated by multiple H-bonds and a π - π stacking interaction [7]. Numerous publications provided experimental data indicating that the lack of the Mg^{2+} co-factor decreases the k_{cat} of dUTPase only by a factor of two [8–12]. Some publications, however, concluded the total inactivity of dUTPase without Mg^{2+} [13–15]. In the latter cases, high concentration of EDTA was used, or the method of providing metal-free conditions was not described.

To investigate the underlying cause of this controversy, we studied the effect of EDTA on dUTP hydrolysis catalysed by two different dUTPases (from *Homo sapiens*, hDUT, UniProt ID: P33316); and from *Mycobacterium tuberculosis*, mtDUT, UniProt ID: P9WNS5) in Mg^{2+} -free conditions. We observed kinetic inhibition by EDTA in the absence of Mg^{2+} . We then measured direct binding of EDTA to dUTPases and 5 other enzymes (including another dNTP pool sanitizing enzyme [16,17] and a DNA polymerase) using isothermal titration calorimetry. Our results show that EDTA binds selectively to the nucleotide binding pocket of dNTP processing enzymes. To understand the structural basis of this specific binding, we took a computational approach and explored the interactions of EDTA within the active site of dUTPases. We found that EDTA develops similar interactions with the protein to those of the cognate substrate.

2. Materials and Methods

2.1. Reagents

We used our previously cloned N-terminally His-tagged dUTPases of human (hDUT and A98F hDUT) and of *Mycobacterium tuberculosis* origin (mtDUT). The *Escherichia coli* MutT (EcMutT) plasmid was a kind gift of Umesh Varshney, Indian Institute of Science, Bangalore, India. These proteins were expressed and purified as described previously [17–20]. We also used TEMpase Hot Start DNA polymerase from VWR (Radnor, PA, USA), a modified *Thermus aquaticus* originating DNA polymerase (Taq polymerase). This protein was heat activated for 15 min at 95 °C before the ITC measurement. Furthermore, we used our previously cloned N-terminally His-tagged *Staphylococcus aureus* uracil glycosylase inhibitor (SaUGI) [21] and *Petroselinum crispum* phenylalanine ammonia-lyase (PcPAL) [22] proteins. The rabbit skeletal myosin subfragment-S1 was a kind gift of Máté Gyimesi, Eötvös University, Budapest, Hungary. These proteins were expressed and purified as described previously [23–25]. The proteins were dialyzed against a buffer pH 7.5 comprising 20 mM HEPES, 100 mM NaCl and 1 mM TCEP. Protein concentration was determined by UV absorbance ($\epsilon_{280} = 10430 \text{ M}^{-1}\text{cm}^{-1}$ for hDUT, $\epsilon_{280} = 15930 \text{ M}^{-1}\text{cm}^{-1}$ for A98F hDUT, $\epsilon_{280} = 2980 \text{ M}^{-1}\text{cm}^{-1}$ for mtDUT, $\epsilon_{280} = 28990 \text{ M}^{-1}\text{cm}^{-1}$ for EcMutT, $\epsilon_{280} = 112760 \text{ M}^{-1}\text{cm}^{-1}$ for Taq polymerase, $\epsilon_{280} = 21890 \text{ M}^{-1}\text{cm}^{-1}$ for SaUGI and $\epsilon_{280} = 45,840 \text{ M}^{-1}\text{cm}^{-1}$ for PcPAL) or using the Bradford assay and is given in monomers. Other reagents were from Sigma-Aldrich (St. Louis, MO, USA).

2.2. ICP-OES

The Mg content of the solutions used in our experiments was determined by inductively coupled plasma optical emission spectrometry. Instrument settings were Labtest Plasmalab ICP spectrometer with 40 element vacuum polychromator, wavelength: 279.553 nm, 27 MHz Ar-Ar plasma, forward power: 1.3 kW, sample introduction with V-groove nebulizer at 2.8 mL/min sample flow rate. Limit of quantitation for Mg was 0.001 mg/L (0.04 μ M).

2.3. Photometric Enzyme Activity Measurement

Continuous pH indicator-based assays were performed to measure enzyme activity at 20 °C as described in [26]. Briefly, 1 μ M protein was used in a buffer pH 7.5 containing 1 mM HEPES, 100 mM KCl and 40 μ M phenol red. A Specord 200 (Analytic, Jena, Germany) spectrophotometer and 10-mm-path length cuvettes were used, and absorbance was recorded at 559 nm. Initial velocity was determined from the first 10% of the progress curve. To explore the inhibitory effect of EDTA on both enzymes, we added this compound to the reaction mixtures at 30 and 100 μ M concentration for hDUT and at 300 μ M concentration for mtDUT. Data fitting was accomplished using OriginPro 7.5 (OriginLab Corp, Northampton, MA, USA).

2.4. Thermofluor Stability Assay

Solutions of 40 μ M (0.8 mg/mL) protein in 20 mM HEPES pH 7.5, 100 mM NaCl, 10 mM β -ME also containing 1000x dilution of Sypro[®] Orange supplemented either with 5 mM MgCl₂ or 100 μ M EDTA were added to the wells of a 96-well thin-wall ABgene[®] PCR plate (Thermo Fisher Scientific, Waltham, MA, USA). Apo enzyme, dUPNPP-complexed and dUMP-complexed enzymes were tested with the addition of saturating concentration of the ligand (100 μ M dUPNPP or 1 mM dUMP) where applicable. The plates were sealed with ABgene[®] Adhesive PCR Plate Sealing Tape (Thermo Fisher Scientific, Waltham, MA, USA) and heated in a Mx3000Pro QPCR System (Agilent Technologies, Santa Clara, CA, USA) from 25 to 90 °C. Fluorescence changes in the wells of the plate were monitored simultaneously with a photomultiplier tube (PMT). The wavelengths for excitation and emission were 492 and 516 nm, respectively.

2.5. Protein and Ligand Preparation Procedure for Molecular Docking

The protonation states of the titratable groups were determined by means of the ProPka algorithm [27,28] at pH 7.4, and the optimization of H-bonding interactions was performed using the PDB2PQR program package version 2.1.1 [29]. The original dUPNPP ligand in both human and *Mycobacterium tuberculosis* dUTPase crystal structures (PDB IDs: 3EHW, under publication in a separate paper and 2PY4 [20], respectively) was manually modified to dUTP.

The structure of the ligand (both EDTA and EDTA-Mg²⁺ complex) was taken from that of 1ZLQ [30]. The Fe³⁺ ion was replaced by a Mg²⁺ ion, and the coordination complex with EDTA was prepared manually using the Molecular Operating Environment 2007.09 program package (Chemical Computing Group, Montreal, Canada) [31]. Subsequent minimization was performed using the MMFF94x force field [32–36]. Gasteiger charges [37] were assigned to the enzyme and to the ligand using the same software.

2.6. Molecular Docking

Docking calculations were performed by means of the AutoDock version 4.2.3 software [38] using default settings and parameters as follows. The protein was kept rigid in the calculations and the ligand was allowed to be flexible. Lennard-Jones parameters 12–10 and 12–6 were used for modelling H-bonds and van der Waals interactions, respectively. To calculate the electrostatic grid map, the distance-dependent dielectric constant of Mehler and Solmayer was utilized. The Lamarckian Genetic Algorithm [39] with the pseudo-Solis and Wets method was used in the docking procedure,

with 300 individuals in the population. The stopping criterion was defined by setting the total number of energy evaluations to 2.0×10^7 . The translation step was set to 5 Å/step, and in both quaternion and torsion steps 5.0 degrees/step was applied. The docking procedure was performed 25×16 (400) times for each enzyme-ligand complex.

Both blind docking [40,41] and active site docking calculations were performed. In blind docking, the grid box was centered on the whole protein and the number of grid points was set to $176 \times 144 \times 176$ for both hDUT and mtDUT. In active site docking, the grid box was centered on the geometric center of dUTP and was large enough to accommodate the dUTP. The number of grid points was set to $42 \times 34 \times 46$ and $46 \times 34 \times 38$ for hDUT and mtDUT, respectively. The lattice point distance was set to 0.375 Å for every docking calculation.

2.7. Determination of the Enzyme-Ligand Interaction Network

The 'Ligand interactions' module [42] of MOE 2007.09 (Chemical Computing Group, Montreal, Canada) [31] was used for the 2D depiction of enzyme ligand interactions. The algorithm to determine the interaction sites in the 'Ligand interactions' module includes the following considerations: (1) Only heavy atom distances are considered; (2) first those residues are determined as interaction sites which are in a 4.5 Å proximity of any ligand atoms; (3) thereafter the distance limit is increased by 0.1 Å, and a new residue is determined as possible site if at least 2 atoms of that residue are within the new distance criteria; (4) increasing the distance by 0.1 Å and the number of the interacting atom by 1, this step is repeated 10 times. The possible H-bond interactions are determined by applying a scoring function. The strength of the H-bond is expressed as percentage probability. We applied a 10% cut-off in identifying possible H-bond interactions.

2.8. Isothermal Titration Calorimetry (ITC) Measurement

ITC experiments were carried out at 293 K on a Microcal ITC₂₀₀ instrument (Malvern Instruments, Malvern, UK), following previously described experimental design [43]. The proteins were dialysed against a buffer pH 7.5 comprising 20 mM HEPES, 100 mM NaCl and 1 mM TCEP. We used 10–250 µM enzyme (hDUT, A98F hDUT, mtDUT, EcMutT, Taq polymerase) in the cell and 70–500 µM EDTA or 500–1500 µM dUPNPP in the syringe. For SaUGI, PcPAL and rabbit myosin S1, 20–80 µM enzyme was used in the cell and 40–120 µM EDTA in the syringe. Next, 5 mM MgCl₂ was used in the syringe to titrate 500 µM EDTA in the cell. Protein concentrations correspond to subunits. Enzymes were also titrated with buffer to consider mixing and dilution heat effects. The titrations were performed with the injection syringe rotating at 750× rpm (and at 200× rpm for mtDUT). A series of 20 injections spaced 180 s apart from each other was performed with injection volumes 0.5 µL for the first and 2 µL for the subsequent 19 injections. All measurements were carried out in duplicates.

The integration of the obtained isotherms was performed using NITPIC v1.2.5 [44] and the global analysis was performed using SEDPHAT v12p1b [45,46]. The fitting model in SEDPHAT was A + B to AB heteroassociation (1:1 binding model), thereby obtaining stoichiometry (n), apparent binding affinity (K_a) and enthalpy change (ΔH) parameters. The fitting was followed by export to GUSSE v1.3.2 to plot the processed data for publication-quality figure preparation [47].

2.9. Figures

Kinetic and thermostability graphs were prepared using OriginPro 7.5 (OriginLab Corp., Northampton, MA, USA). ITC graphs were prepared by GUSSE v1.3.2 [47]. Ligand interaction network images were prepared by MOE 2007.09 [31]. Structural images were prepared using the Visual Molecular Dynamics package [48] or the PyMOL Molecular Graphics System, Version 2.0 Schrödinger, LLC (New York, NY, USA) [49].

3. Results

3.1. Assessment of the Mg^{2+} Content of the Assay Solutions

To be able to measure the specific effects of EDTA, we needed to establish Mg^{2+} -free or low Mg^{2+} concentration conditions without the use of EDTA. Therefore, we used high purity reagents and measured the exact Mg content of our buffers with atomic spectroscopy. The high sensitivity inductively coupled plasma optical emission spectrometry yields a quantitation limit of 0.001 mg/L for any oxidation state of Mg. The Mg content of our dH_2O , dialysis buffer and dUTP nucleotide stock fell under the quantitation limit. The concentration of other divalent or trivalent metals (Mn, Ni, Co, Cr, Sr) that could potentially complement the function of Mg^{2+} fell under the quantitation limit, as well. However, the Mg content of our activity assay buffer was measured to be 0.007 ± 0.00014 mg/L ($0.3 \mu M$) despite the fact that we purchased the finest chemicals available. The smallest reported dissociation constant for the $ATP:Mg^{2+}$ complex is $46.3 \mu M$ [50]. We considered this value to calculate the equilibrium concentration of the $dUTP:Mg^{2+}$ complex possibly present in our reaction mixtures. As we used a range of 2–90 μM dUTP in our kinetics measurements, the calculated concentrations of the $dUTP:Mg^{2+}$ complex were 0.02–0.4 μM in the solutions, i.e., at most 1% of the total dUTP was complexed with Mg^{2+} in our assays.

3.2. EDTA Decreases Enzyme Activity

We measured the dUTP hydrolysing activity of hDUT and mtDUT in the presence of Mg^{2+} (reported previously [20,51]) or EDTA and in the absence of both compounds (Figure 1, Table 1). In the absence of Mg^{2+} , the activity decreased to 70% and 33%, while the K_M increased with 10% (within experimental uncertainty) and 50% for hDUT and mtDUT, respectively. The relatively modest change in the kinetic parameters upon lowering the Mg^{2+} concentration close to zero was not unexpected. We previously investigated the reaction mechanism of these enzymes using transient kinetics and QM/MM methods and found that the primary role of the Mg^{2+} in this system is to enforce a coordination constraint upon the enzyme–substrate complex which drives the reaction towards the transition state [51,52]. The rate-limiting proton-transfer reaction during hydrolysis is not directly dependent on the Mg^{2+} ion and therefore, a complete abolishment of the reaction is not expected in the absence of Mg^{2+} [52]. What was unexpected, however, is that the addition of EDTA further perturbed the enzyme kinetic parameters (Figure 1, Table 1). hDUT was inhibited even by as low as 30 μM EDTA so that the K_M increased 2.7-fold. 100 μM EDTA practically abolished the activity decreasing the k_{cat} to 6%. mtDUT was adversely affected by only higher concentrations of EDTA (300 μM) increasing the K_M 3.7-fold compared to that measured in the absence of Mg^{2+} and EDTA (Table 1).

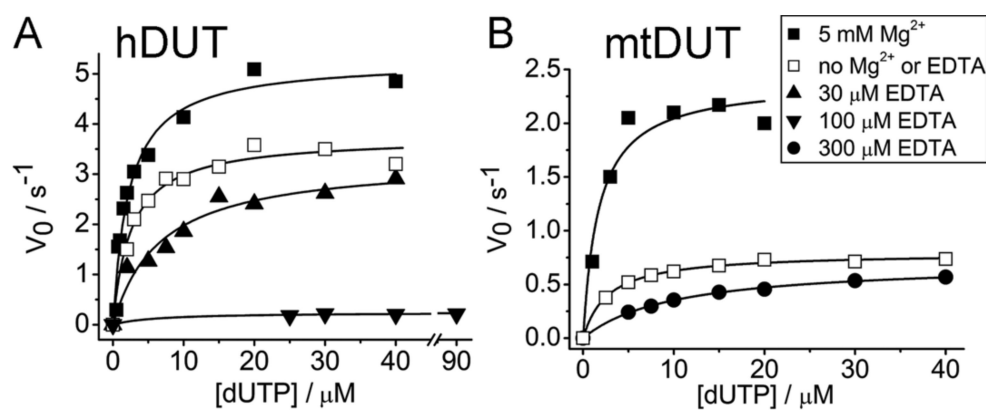


Figure 1. EDTA inhibits the enzyme activity of dUTPase. Figure shows Michaelis-Menten curves of hDUT (A) and mtDUT (B) in Mg^{2+} -saturated condition (solid square), without Mg^{2+} or EDTA (open square) and in the presence of EDTA (solid triangles and circle). K_M and k_{cat} values of the fitted datasets can be found in Table 1.

Table 1. Kinetic parameters of hDUT and mtDUT in the presence of Mg²⁺ or EDTA or in the absence of both.

	hDUT		mtDUT		
	k _{cat} /s ⁻¹	K _M /μM	k _{cat} /s ⁻¹	K _M /μM	
5 mM Mg ²⁺ , no EDTA	5.27 ± 0.24	2.26 ± 0.33	5 mM Mg ²⁺ , no EDTA	2.39 ± 0.16	1.72 ± 0.51
No Mg ²⁺ , no EDTA	3.71 ± 0.12	2.49 ± 0.37	No Mg ²⁺ , no EDTA	0.79 ± 0.01	2.70 ± 0.18
30 μM EDTA, no Mg ²⁺	3.30 ± 0.26	6.72 ± 1.69	300 μM EDTA, no Mg ²⁺	0.71 ± 0.01	10.04 ± 0.50
100 μM EDTA, no Mg ²⁺	0.24 ± 0.03	6.16 ± 5.34			

The increase in K_M suggests competitive inhibition, meaning that EDTA competes with the ligand for the same binding site. Decreasing k_{cat} indicates non-competitive inhibition, i.e., the inhibitor binds to somewhere else other than the active site. Our results suggest that EDTA binds to the active site of both hDUT and mtDUT and it may additionally bind to other binding site(s), as well. The calculated 1–0.44% dUTP:Mg²⁺ content of the total dUTP present throughout the measured concentration range clearly does not account for the relatively high, 70% and 33% residual activity obtained for hDUT and mtDUT, respectively. Thus, these results strengthen the observations reported in [8–11] that Mg²⁺ or other divalent metal ions only increase, not enable, the hydrolytic activity of dUTPase roughly by a factor of two.

3.3. EDTA Does Not Destabilize the Enzyme

To exclude possible detrimental effects of EDTA on the structural stability of dUTPases, we measured the melting temperatures of hDUT in the presence of 5 mM MgCl₂, of 100 μM EDTA or in the absence of both (Figure 2, Table 2). We chose hDUT as the steady state kinetic experiments showed that EDTA has a greater effect on hDUT than on mtDUT. The thermofluor data revealed that the thermostability of the enzyme is similar in the presence and absence of EDTA (Table 2). In the presence of Mg²⁺, the melting temperatures of the apo, dUMP and dUPNPP complexed enzymes increase with 0.9, 2.6 and 3.8 °C, respectively (Table 2). These results suggest that Mg²⁺ stabilizes the protein, especially when complexed with the substrate analogue or with the product. The results also suggest that EDTA does not have an effect on enzyme stability that could account for the largely decreased activity.

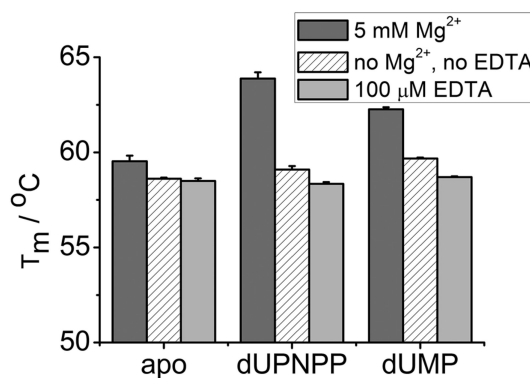


Figure 2. Melting temperatures of hDUT in the presence and absence of Mg²⁺ and EDTA. The apo enzyme and both complexes with the substrate analogue dUPNPP and the product dUMP were measured in Mg²⁺-saturated condition (dark gray), without Mg²⁺ or EDTA (white with stripes) and in the presence of EDTA (light gray). Calculated melting temperatures can be found in Table 2.

Table 2. Melting temperatures of hDUT obtained by thermofluor assay.

	T_m (5 mM Mg^{2+})/°C	T_m (No Mg^{2+} , no EDTA)/°C	T_m (100 μ M EDTA)/°C
apo	59.5 \pm 0.3	58.6 \pm 0.1	58.5 \pm 0.1
dUPNPP	63.9 \pm 0.3	59.1 \pm 0.2	58.3 \pm 0.1
dUMP	62.3 \pm 0.1	59.7 \pm 0.1	58.7 \pm 0.1

3.4. Blind Docking Indicates EDTA Binding to the Surface and the Active Site of Both dUTPases

To identify potential binding sites of EDTA on the dUTPase enzyme, we chose to apply blind docking to both hDUT (PDB ID: 3EHW) and mtDUT (PDB ID: 2PY4 [20]) using the AutoDock 4.2.3 program package [38]. In these calculations, the whole protein structure is considered as potential binding surface, thus the ligand can explore distinct binding cavities and modes, as well. The blind docking calculations were performed 400 times for both EDTA and dUTP ligands. Among these runs, EDTA recognized the orthosteric binding site in hDUT and mtDUT 1 and 18 times, respectively. In the remaining cases, the surface of the protein was identified as EDTA recognition site (Figure 3). For comparison, the physiological substrate dUTP bound to the orthosteric cavity 5 and 22 times in hDUT and mtDUT, respectively. Thus, the obtained small numbers of orthosteric cavity exploration by EDTA could still represent effective binding to the active site. The difference in the number of active site bound ligands in hDUT and mtDUT might originate from the difference in their surface polarity. 16.3% and 10.1% of the protein surface is positively charged (arginine or lysine residues) in hDUT and in mtDUT, respectively. In effect, the larger basic surface in hDUT can result in more frequent binding on the surface of the protein by the negatively charged EDTA and dUTP. These results suggest that EDTA binds both to the surface and the active site of the dUTPase enzyme.

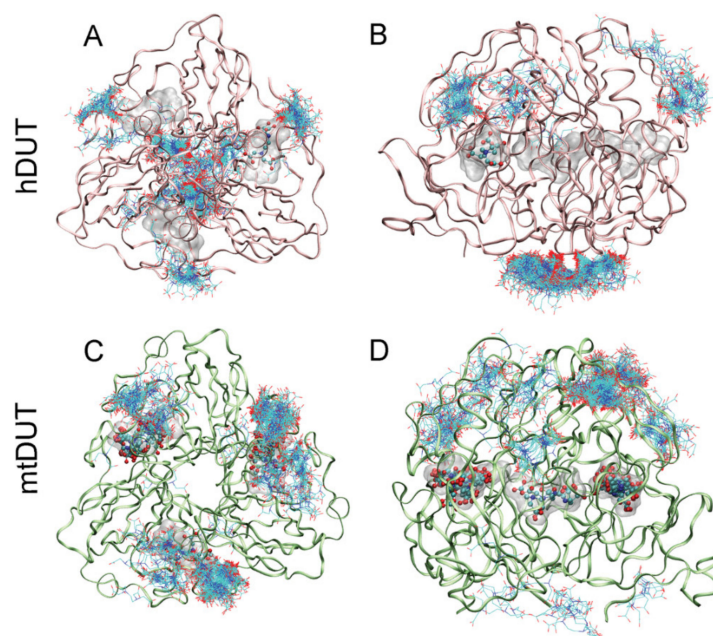


Figure 3. Blind docking of EDTA to dUTPase enzymes. Figures show all 400 docked EDTA molecules to hDUT (A,B) and mtDUT (C,D). Panels B and D show the same structure as A and C, respectively, upon rotating the protein by 90°. The active sites of dUTPases contain bound dUTP represented with the transparent space filling method (Maximal Speed Molecular Surfaces [53]). EDTA molecules bound to the active site are shown with ball and stick representation, whereas EDTA molecules bound to the surface of the enzyme are shown as only stick representation. Protein backbone is shown as pink and green ribbon for hDUT and mtDUT, respectively.

3.5. Molecular Docking Suggests That Nucleotide and EDTA Share Common Interaction Points Within the Active Site

To investigate the binding conformation of EDTA in the active site of dUTPase, we performed active site docking. For comparison, docking with the cognate ligand, dUTP, was also performed to the same protein structures. The accuracy and reliability of the docking simulation is confirmed by the low RMSD values (0.001 Å for both mtDUT and hDUT) comparing the docked dUTP to the dUPNPP within the crystal structure. The low RMSD value implies that the docking process reproduced the location and the conformation of the physiological ligand in the crystal structures. Figure 4 shows that the physiological ligand, dUTP, and EDTA explore the same space within the active site. In particular, EDTA overlaps with the phosphate chain and the sugar in both structures and in hDUT, EDTA also overlaps with the uracil ring of the physiological ligand. We also performed docking of the EDTA:Mg²⁺ complex to the dUTPase active sites and obtained ΔG_{bind} values close to zero. This implies that this complex is unlikely to productively bind to the active site and emphasizes the role of the free negative charges and/or the flexibility of EDTA in its interaction with the assayed proteins.

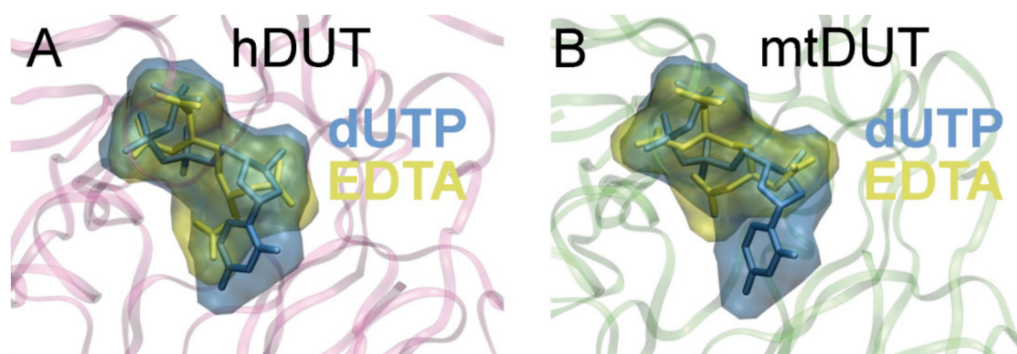


Figure 4. Molecular docking shows that EDTA occupies the same binding site in the dUTPase active site as the cognate ligand, dUTP. The Maximal Speed Molecular Surfaces [53] of dUTP (blue) and EDTA (yellow) largely overlap in both (A) hDUT and (B) mtDUT. Both ligands are also shown as stick representation besides the transparent surface representation. Protein backbone is shown as pink and green ribbon for hDUT and mtDUT, respectively.

We also mapped the secondary interactions within the enzyme-EDTA complexes and compared this interaction network to that of the enzyme:dUTP complexes (Figure 5.). The H-bonding interactions in particular are compiled in Table 3. All of the residues predicted to interact with EDTA are found in one of the five conserved motifs present in all dUTPases [6]. Arg85/64 (amino acid numbering in hDUT and mtDUT, respectively), Asp102/83 and Arg153/140 are key and conserved amino acids in the binding site and were predicted as anchor points in EDTA binding, too. These residues are responsible for the coordination of the catalytic water (Asp102/83) and of the phosphate chain [54–56]. Two important residues in binding the γ -phosphate of the nucleotide substrate, Ser160/147 and Thr161/Ser148 [56,57] were determined to be key participants in the enzyme–EDTA interaction as well. These shared anchor points suggest that EDTA binds to the same site within the enzyme active site as the physiological substrate dUTP.

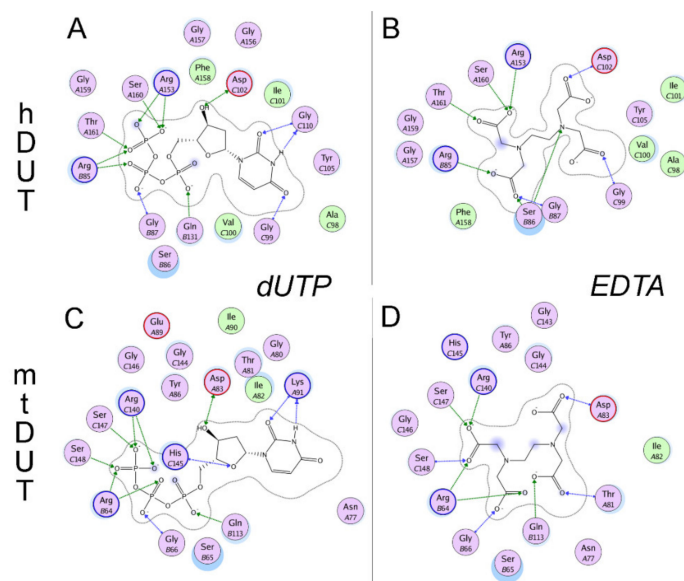


Figure 5. Comparison of the interaction networks between dUTPase:dUTP and dUTPase:EDTA complexes obtained by docking. (A) hDUT:dUTP complex, (B) hDUT:EDTA complex representing the most populated structure from active site docking, (C) mtDUT:dUTP complex, (D) mtDUT:EDTA complex representing the most populated structure from active site docking. Residues shown are within 5.4 Å from the ligand potentially interacting with it as determined by the ‘Ligand interactions’ algorithm [42] of MOE 2007.09 [31]. Color coding is as follows: Lilac background, polar residue; green background, apolar residue; blue border, basic residue; red border, acidic residue; blue halo, solvent accessible residues; blue smudge, solvent accessible atoms of the ligand; green arrow, H-bonds with residue side chain; blue arrow, H-bonds with residue backbone. No Mg^{2+} ions were present in this docking simulation. Ionic interactions between arginine sidechains and the phosphate chain of dUTP or the acetate part of EDTA were treated as H-bonds by the algorithm.

Table 3. H-bonding interaction points between dUTPase enzymes and EDTA or dUTP according to the active site dockings.

hDUT		mtDUT	
EDTA	dUTP	EDTA	dUTP
Arg85 (II)	Arg85 (II)	Arg64 (II)	Arg64 (II)
Ser86 (II)			
Gly87 (II)	Gly87 (II)	Gly66 (II)	Gly66 (II)
Gly99 (III)	Gly99 (III)		
		Thr81 (III)	
Asp102 (III)	Asp102 (III)	Asp83 (III)	Asp83 (III)
	Gly110 (III)		Lys91 (III)
	Gln131 (IV)	Gln113 (IV)	Gln113 (IV)
Arg153 (V)	Arg153 (V)	Arg140 (V)	Arg140 (V)
			His145 (V)
Ser160 (V)	Ser160 (V)	Ser147 (V)	Ser147 (V)
Thr161 (V)	Thr161 (V)	Ser148 (V)	Ser148 (V)

Roman numerals in parenthesis represent the adequate conserved motifs, rows represent identical positions in the 3D structure [6].

3.6. Isothermal Titration Calorimetry Data Directly Prove EDTA Binding to the Nucleotide Binding Pocket of dUTPase

We used isothermal titration calorimetry (ITC) to obtain direct proof of EDTA binding to dUTPases. Figure 6 shows titrations of the human and mycobacterial dUTPases (panels A and B, respectively) with EDTA. The titration curves indicate exothermic binding between dUTPases and EDTA in the absence of Mg^{2+} ion. The thermodynamic parameters indicate strong binding with the K_d in the nanomolar range (199 nM for hDUT, and 78 nM for mtDUT) (Table 4). As our *in silico* results indicated that EDTA binds to the active site of dUTPases, we aimed to investigate this hypothesis *in vitro*. Thus, we performed the ITC measurement using an active site mutant of dUTPase. The previously described A98F hDUT mutant excludes dUTP from its active site as the phenyl ring of the F98 residue occupies the space of the uracil ring of dUTP [19]. As shown by the docking of EDTA to hDUT in Figure 4A, the binding site of EDTA overlaps with that of the uracil ring. Therefore, we expected that EDTA binding to the A98F hDUT mutant would be compromised if EDTA binding occurs in the dUTP binding pocket. The ITC titration of A98F hDUT with EDTA clearly shows that the active site mutant hDUT lost its EDTA binding capacity (Figure 6C). Thus, we concluded that EDTA binding to dUTPase primarily occurs in the nucleotide binding pocket.

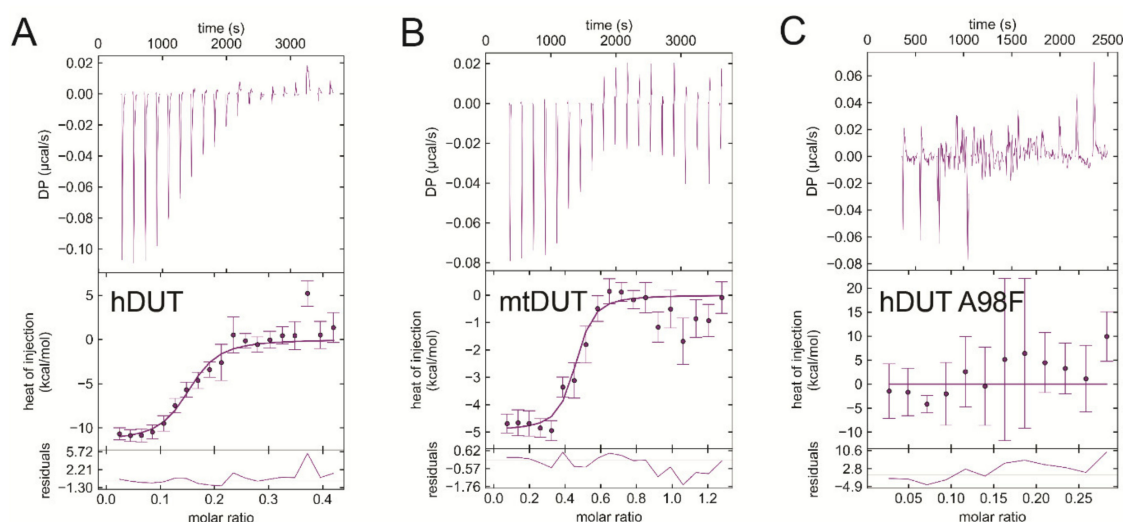


Figure 6. Isothermal titration calorimetry (ITC) titrations of wild-type and active-site mutant dUTPases with EDTA prove strong and direct EDTA binding to the active site. (A) hDUT titrated with EDTA. (B) mtDUT titrated with EDTA. (C) Titration of the A98F hDUT mutant with EDTA shows no binding between the molecules. Titrations were carried out at pH 7.5 and at 293 K.

Table 4. Thermodynamic parameters yielded by the analysis of the ITC measurements. K_d values are apparent dissociation constants at pH 7.5 and at 293 K. Values shown are averages and standard deviations.

Titrand	Titrant	$\Delta H/\text{kcal/mol}$	$-T\Delta S/\text{kcal/mol}$	$\Delta G/\text{kcal/mol}$	$K_d/\mu\text{M}$
hDUT	EDTA	-11.2 ± 0.4	2.2 ± 0.4	-9.0 ± 0.0	0.20 ± 0.009
hDUT	dUPNPP	-17.4 ± 3.6	11.5 ± 3.7	-5.9 ± 0.2	43.9 ± 14.6
mtDUT	EDTA	-4.2 ± 1.0	-5.3 ± 1.2	-9.6 ± 0.2	0.078 ± 0.023
mtDUT	dUPNPP	-4.5 ± 0.2	-2.1 ± 0.4	-6.6 ± 0.6	13.9 ± 11.7
EDTA	Mg^{2+}	4.4 ± 0.3	-12.5 ± 0.6	-8.0 ± 0.9	2.53 ± 0.18
EcMutT	EDTA	-9.7 ± 0.02	1.3 ± 0.1	-8.4 ± 0.1	0.55 ± 0.066
Taq polymerase	EDTA	-6.3 ± 0.7	-3.5 ± 0.7	-9.8 ± 0.0	0.047 ± 0.001

As a control, we titrated the dUTPases with their practically non-hydrolysable substrate analogue dUPNPP in the absence of Mg^{2+} ion. Both hDUT and mtDUT exhibited exothermic dUPNPP binding (Supplementary Figure S1A,B, respectively). The obtained K_d value for the hDUT:dUPNPP complex is 44 μ M. The same titration in the presence of Mg^{2+} has previously been done yielding K_d values between 2–7 μ M [7,18,51]. Taking into consideration that Mg^{2+} supports a more favorable charge distribution within the substrate-bound active site [52], the obtained one order of magnitude increase in the K_d values without Mg^{2+} is reasonable.

We also performed EDTA titrations with Mg^{2+} as a control (Figure 7A). Mg^{2+} binding to EDTA proved to be an endothermic reaction well separable from EDTA binding to dUTPases. The dissociation constant of the complex is around 3 μ M confirming literature data [58]. We performed a further control measurement, where we added extra Mg^{2+} into the buffer of hDUT and then titrated with EDTA (Figure 7B). Here we observed a mixed binding curve, suggesting that the exothermic binding of EDTA to the enzyme and the endothermic binding of EDTA to Mg^{2+} take place at the same time. As this curve is much different from the EDTA-hDUT or EDTA-mtDUT binding curves (Figure 6A,B), we could rule out the possibility of measuring the binding of potential residual Mg^{2+} .

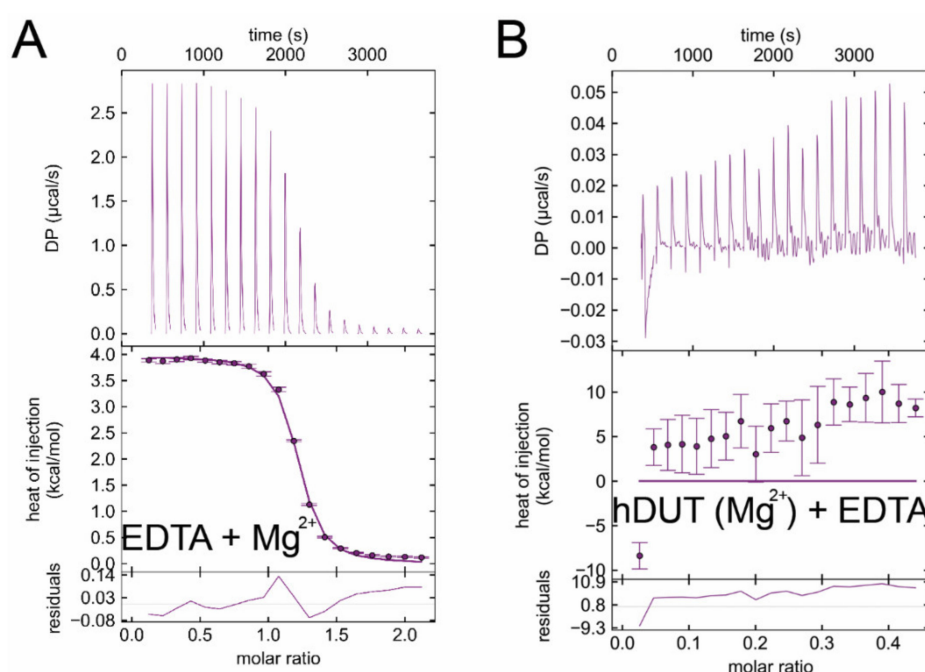


Figure 7. Control ITC measurements. **(A)** ITC titration of EDTA with $MgCl_2$. **(B)** ITC titration of hDUT with additional 5 mM $MgCl_2$ in the buffer with EDTA. Titrations were carried out at pH 7.5 and at 293 K.

3.7. EDTA Binds to *Taq* Polymerase and *MutT*, Two Additional dNTP Processing Enzymes

As EDTA occupied the dNTP binding site in both dUTPases investigated, we hypothesized that EDTA could bind other dNTP processing enzymes, as well. We selected two more enzymes, the *Escherichia coli* MutT (EcMutT) exhibiting 8-oxo-dGTPase activity [17] and the *Thermus aquaticus* DNA polymerase (*Taq* polymerase) [59] to test their ability to bind EDTA. Figure 8A shows the ITC curve of EcMutT and EDTA binding in the absence of Mg^{2+} . Interestingly, the interaction of EDTA with EcMutT shows similar characteristics to that with dUTPases (Table 4). It is worth mentioning that EcMutT is a promiscuous enzyme which hydrolyses other dNTPs including dGTP, dCTP, dTTP, and dUTP beside 8-oxo-dGTP [60]. The *Taq* polymerase exhibits the strongest measured exothermic binding to EDTA in the absence of Mg^{2+} ($K_d = 47$ nM, Figure 8B, Table 4). This enzyme promiscuously processes all dNTPs.

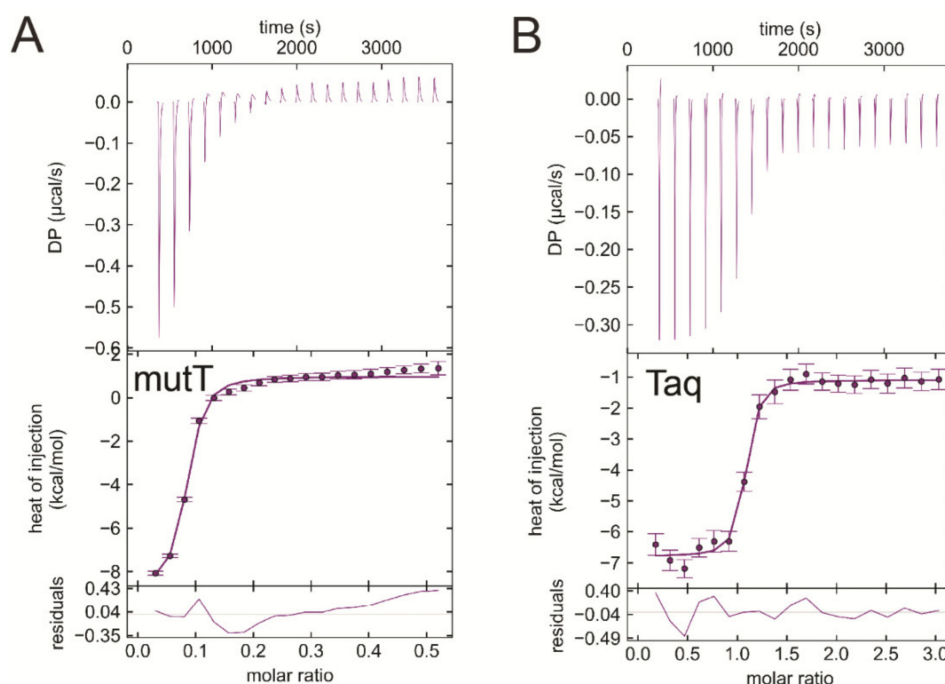


Figure 8. ITC titration of various dNTP hydrolyzing proteins with EDTA (A) EcMutT titration with EDTA. (B) *Thermus aquaticus* DNA polymerase titration with EDTA represents strong binding between the reactants. Titrations were carried out at pH 7.5 and at 293 K.

We also tested enzymes that either have an ATP binding site (skeletal myosin S1) or have no nucleotide binding site at all (uracil glycosylase inhibitor and phenylalanine ammonia-lyase). As Supplementary Figure S2 shows, these proteins not having a dNTP binding pocket do not interact with EDTA in the ITC measurements.

4. Discussion

The controversy in the literature about dUTPase activity in the absence of metal(II) ions brought our attention to a putative, novel effect of EDTA on hydrolytic activity. We show, in effect, that EDTA competes with dUTP for the active site. EDTA is commonly used in biochemical experiments to establish metal-free conditions. However, EDTA has previously been reported to exhibit inhibitory effect on various types of enzymes via partially known (competitive inhibition of human liver arginase [61], electron donor in the reactions catalyzed by veratryl alcohol oxidase [62], and horseradish peroxidase [63,64]) or unknown mechanisms (prenyltransferase MaPT [65], peptidase activity of the angiotensin-converting enzyme [66]). Furthermore, a series of ethylenediamine-based farnesyltransferase inhibitors has been developed and evaluated as antimalarial and anticancer agents [67,68]. Nevertheless, the multifactorial effect of EDTA on enzymes has not penetrated the scientific community. Now that we show potent interaction with enzymes playing key cellular roles including a DNA polymerase and DNA repair enzymes, the view of EDTA being an inert biochemical reagent will hopefully be shifted.

EDTA inhibited the Mg^{2+} -free dUTP hydrolysis activity of both dUTPases with similar mechanism but to a different degree (cf. Table 1). This observation is consistent with the results of the docking simulations and of the ITC measurements. We found that the inhibition comprises of a competitive and a non-competitive element in both dUTPases. The ITC experiments and the docking simulations showed that EDTA binds to the active site of dUTPase directly competing with the physiological substrate dUTP (Figures 4–6). EDTA assumes somewhat different conformations though in the two different active sites despite the fact that the conformations of the dUTP ligand in the two structures are identical. The analysis of the interaction network within the EDTA bound active sites of hDUT and

mtDUT also shows some differences (Table 3, Figure 5). However, the fact that EDTA exhibited strong interaction with four different dNTP hydrolyzing enzymes and no interaction with an ATPase calls our attention to enzyme residues that are responsible for the specificity of the nucleotide sugar (i.e., ribose (NTP) or 2' deoxyribose (dNTP)). Taking a closer look at the protein environment of the C2' atom of the bound nucleotide in all five of these enzymes (Figure 9), it is visible that the dNTP-specific enzymes (i.e., dUTPases, Taq, and MutT) sterically ensure the exclusion of the 2'OH while the NTP-specific enzyme, myosin does not. The residues shown in Figure 9 are responsible for the discrimination of the nucleotide sugars and are conserved in dUTPases [6] and in DNA polymerase I enzymes [69] and at least partially conserved in MutT (Figure S3). In the two dUTPases investigated, the same residues are involved in the interaction with EDTA (Figure 5, Ile101/82 and Tyr105/86).

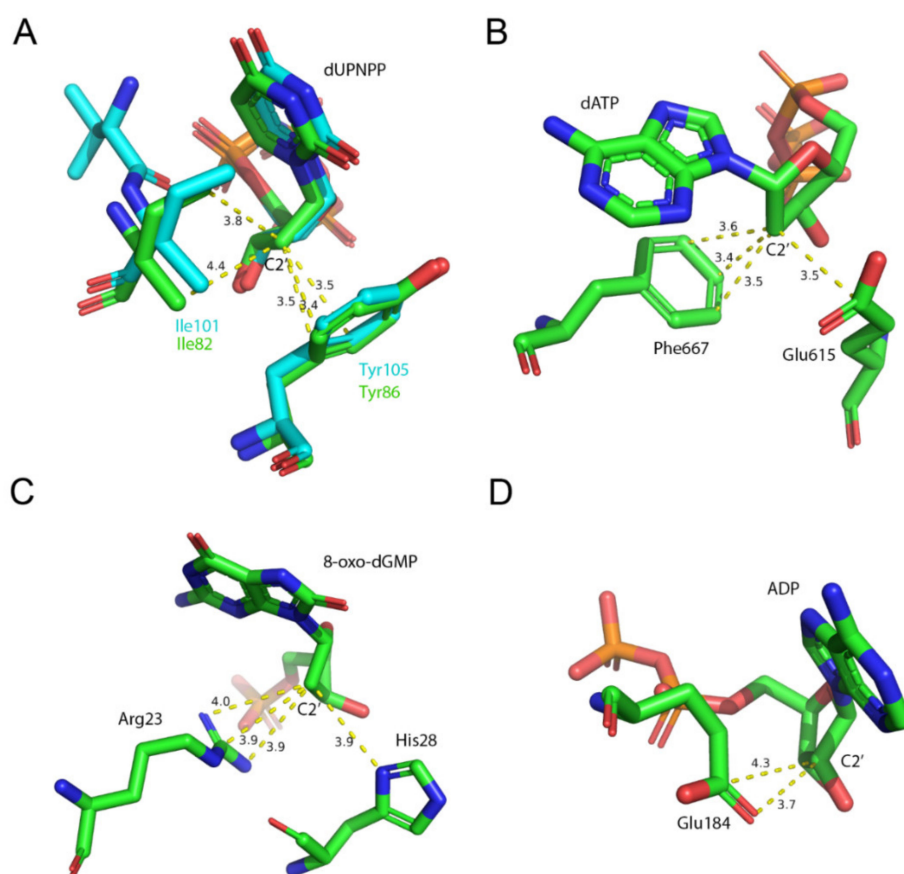


Figure 9. Molecular environment of the C2' atom of the nucleotide within the active sites of the investigated (d)NTP hydrolyzing enzymes. Residues within 4 Å of C2' are shown. (A) mtDUT (green, PDB ID: 2PY4 [20]) aligned with hDUT (cyan, PDB ID: 3EHW) both in complex with the non-hydrolysable dUTP analogue, dUPNPP. The conserved Ile and Tyr residues exclude a potential hydroxyl group on 2C' atom. (B) The C2' atom of the nucleotide within the Taq polymerase (PDB ID: 6Q4V [70]) fits in a sterically restricted environment. (C) *E. coli* MutT in complex with the hydrolysis product 8-oxo-dGMP (PDB ID: 3A6T [71]). A potential hydroxyl group on C2' atom is similarly excluded as in the previous two enzymes. (D) Squid myosin S1 in complex with ADP (PDB ID: 3I5F [72]). The C2' atom is sterically restricted from only one direction. The opposite side of the sugar plane faces the solvent.

The striking results showing that EDTA occupies the active site in a manner similar to the nucleotide ligand urged us to obtain EDTA complexed dUTPase crystal structures. We put much effort in crystallization trials and collected several data sets from co-crystallized and soaked crystals as well. However, we could only observe potential molecular details of the acetate groups of EDTA within the

active site of the mtDUT. After several trials, we concluded that EDTA, especially the ethylenediamine moiety might be too flexible to be observed in the crystal phase.

The interaction of EDTA with Mg^{2+} is endothermic while the interaction of EDTA with proteins proved to be exothermic. Thus, the two processes can be clearly separated from each other and any residual Mg^{2+} did not disturb the evaluation of EDTA binding to the proteins. While the EDTA: Mg^{2+} interaction is clearly driven by entropy predominantly due to the metal ion dehydration [73], EDTA binding to the proteins is more enthalpy-driven (Table 4). The relatively small entropy and larger enthalpy contribution to EDTA binding to the enzyme active sites is in accordance with our hypothesis that EDTA remains highly flexible within the active site while engaging in a significant number of secondary interactions with active site residues (Figure 5). Interestingly, the K_d values of the enzyme:EDTA complexes are in the submicromolar range, 1–3 orders of magnitude lower than those of the Mg^{2+} :EDTA or the enzyme:substrate complexes (Table 4) even in the presence of Mg^{2+} (K_d of the (Mg^{2+} :dNTP):enzyme complex being in the tens of micromolar range in Taq [59] and MutT [17], and in the low micromolar range in dUTPases [18,51]).

The blind docking simulations suggested that EDTA may also bind to the surface of the enzyme potentially contributing the observed non-competitive type inhibition. The most populated EDTA binding surface areas differ in hDUT and mtDUT (Figure 3). EDTA seems to preferably bind to one of the entrances of the polar central channel of hDUT (Figure 3 A–B) while it only weakly populates the corresponding apolar area in mtDUT in the docking runs (Figure 3 C–D). Considering the enzymatic mechanism, EDTA binding to the outer central channel may not have great or any effect on the enzymatic activity as this part have not shown significant conformational changes in previous studies [55,74]. On the other hand, EDTA may perturb the interaction of the C-terminal arm with the protein core as this contact surface is the first and second most populated EDTA binding site in mtDUT and hDUT, respectively, in the docking simulations (Figure 3). The intact C-terminal arm–protein core interaction is necessary for the hydrolysis to occur as this interaction provides the shielding of the active site from the solvent [52,57,74]. The differences in the predicted EDTA–protein interactions, especially at the C-terminal arm can explain the observed differences in EDTA-inhibited dUTPase activities between hDUT and mtDUT. Using wild type and active site mutant dUTPases, we have conclusively identified the binding site to be the active site in the ITC measurements (Figure 6) and could not differentiate additional binding sites. The rather non-specific binding predicted on the molecular surface is not expected to be accompanied by a large thermal effect and therefore, the docking and the ITC results do not challenge each other.

The presented results call attention to the possibility that EDTA may be a binding partner/inhibitor of many more dNTP hydrolyzing enzymes. In addition, previous studies have shown that removal of EDTA from buffers might not be straightforward. EDTA is often retained in the dialysis bag even though the pore size is over hundred times larger than the molecule itself and buffer changing does not improve removal efficiency either [75]. Moreover, EDTA was reported to bind to both strong and weak anion exchange resins and to be only eluted at 240 mM NaCl, leading to 10–200 fold enrichment of EDTA in the elute compared to the initial solution [76,77]. Therefore, the common unsuspecting use of EDTA as a metal chelator during enzyme preparation procedures may introduce unwanted effects and misinterpretation of enzyme activity results.

5. Conclusions

In conclusion, we found that EDTA is able to occupy the conserved dNTP binding sites in two dUTPases and potently binds to Taq polymerase and MutT, as well, while not interacting with the myosin ATPase. Our results together with the cited literature call attention to the fact that EDTA has multifactorial effects on several enzymes and therefore, the rethinking of the use of EDTA in enzymatic experiments is necessary. Considering that the chemical synthesis of substituted ethylenediamines is relatively straightforward, we propose that ethylenediamine-based inhibitors could be developed

against DNA polymerases, various DNA repair and other nucleotide hydrolyzing enzymes for use in molecular biology experiments.

Supplementary Materials: The following are available online at <http://www.mdpi.com/2218-273X/9/10/621/s1>, Figure S1: ITC titrations with dUTPases and dUPNPP confirm the functionality of the enzyme, Figure S2: ITC titrations show the lack of binding between EDTA and *Staphylococcus aureus* uracil glycosylase inhibitor, *Petroselinum crispum* phenylalanine ammonia-lyase and rabbit myosin subfragment 1, Figure S3: The alignment of MutT protein sequences indicate that the residues involved in 2' deoxyribose exclusion from the active site are conserved amongst the above species.

Author Contributions: A.L. and E.T. performed the biochemical assays. A.L. and B.J. carried out the docking simulations. É.V.S. performed the ITC measurements. L.B. performed the ICP-OES measurement. I.L. and Á.Á.B. performed crystallography. B.V., B.G.V. and J.T. supervised the experiments. A.L., B.J., É.V.S., and J.T. wrote the manuscript. All authors read and commented on the paper.

Funding: This work was supported by the National Research, Development and Innovation Office [K115993, FK124527, K119493, NVKP_16-1-2016-0020, 2017-1.3.1-VKE-2017-00002, 2017-1.3.1-VKE-2017-00013, VEKOP-2.3.2-16-2017-00013 to BGV, NKP-2018-1.2.1-NKP-2018-00005] and by the BME-Biotechnology FIKP grant (BME FIKP-BIO) of the Ministry of Human Capacities. AL was awarded the 'Students for science' grant of the Sándor Wekerle Foundation. BV thanks for the financial support for the European Union and the Hungarian State, co-financed by the European Regional Development Fund in the framework of the GINOP-2.3.4-15-2016-00004 project, aimed to promote the cooperation between the higher education and the industry. JT is the recipient of the János Bolyai Research Scholarship of the Hungarian Academy of Sciences. Funding for open access charge: Hungarian Scientific Research Funds.

Acknowledgments: The authors thank M. Lábadi for technical support at the HPC Centre of the University of Szeged and Daumantas Matulis for the advice on the melting temperature measurement.

Conflicts of Interest: The authors declare no conflict of interest. The funders had no role in the design of the study; in the collection, analyses, or interpretation of data; in the writing of the manuscript, or in the decision to publish the results.

References

1. Jorgensen, P.L.; Håkansson, K.O.; Karlsh, S.J.D. Structure and Mechanism of Na, K-ATPase: Functional Sites and Their Interactions. *Annu. Rev. Physiol.* **2003**, *65*, 817–849. [[CrossRef](#)] [[PubMed](#)]
2. Sprang, S.R. G Protein Mechanisms: Insights from Structural Analysis. *Annu. Rev. Biochem.* **1997**, *66*, 639–678. [[CrossRef](#)] [[PubMed](#)]
3. Tomkinson, A.E.; Vijayakumar, S.; Pascal, J.M.; Ellenberger, T. DNA Ligases: Structure, Reaction Mechanism, and Function. *Chem. Rev.* **2006**, *106*, 687–699. [[CrossRef](#)] [[PubMed](#)]
4. Rothwell, P.J.; Waksman, G. Structure and mechanism of DNA polymerases. *Advances Protein Chem.* **2005**, *71*, 401–440. [[PubMed](#)]
5. Mildvan, A.S.; Xia, Z.; Azurmendi, H.F.; Saraswat, V.; Legler, P.M.; Massiah, M.A.; Gabelli, S.B.; Bianchet, M.A.; Kang, L.-W.; Amzel, L.M. Structures and mechanisms of Nudix hydrolases. *Arch. Biochem. Biophys.* **2005**, *433*, 129–143. [[CrossRef](#)] [[PubMed](#)]
6. Vértessy, B.G.; Tóth, J. Keeping uracil out of DNA: physiological role, structure and catalytic mechanism of dUTPases. *Acc. Chem. Res.* **2009**, *42*, 97–106. [[CrossRef](#)]
7. Pecsli, I.; Leveles, I.; Harmat, V.; Vértessy, B.G.; Toth, J. Aromatic stacking between nucleobase and enzyme promotes phosphate ester hydrolysis in dUTPase. *Nucleic Acids Res.* **2010**, *38*, 7179–7186. [[CrossRef](#)]
8. Mol, C.D.; Harris, J.M.; McIntosh, E.M.; Tainer, J.A. Human dUTP pyrophosphatase: uracil recognition by a beta hairpin and active sites formed by three separate subunits. *Structure* **1996**, *4*, 1077–1092. [[CrossRef](#)]
9. Kovári, J.; Barabás, O.; Takács, E.; Békési, A.; Dubrovay, Z.; Pongrácz, V.; Zagyva, I.; Imre, T.; Szabó, P.; Vértessy, B.G. Altered Active Site Flexibility and a Structural Metal-binding Site in Eukaryotic dUTPase. *J. Biol. Chem.* **2004**, *279*, 17932–17944. [[CrossRef](#)]
10. Freeman, L.; Buisson, M.; Tarbouriech, N.; Van der Heyden, A.; Labbé, P.; Burmeister, W.P. The Flexible Motif V of Epstein-Barr Virus Deoxyuridine 5'-Triphosphate Pyrophosphatase Is Essential for Catalysis. *J. Biol. Chem.* **2009**, *284*, 25280–25289. [[CrossRef](#)]
11. Mustafi, D.; Bekesi, A.; Vértessy, B.G.; Makinen, M.W. Catalytic and structural role of the metal ion in dUTP pyrophosphatase. *Proc. Natl. Acad. Sci. USA* **2003**, *100*, 5670–5675. [[CrossRef](#)]

12. Kovári, J.; Barabás, O.; Varga, B.; Békési, A.; Tölgyesi, F.; Fidy, J.; Nagy, J.; Vértessy, B.G. Methylene substitution at the α - β bridging position within the phosphate chain of dUDP profoundly perturbs ligand accommodation into the dUTPase active site. *Proteins Struct. Funct. Bioinforma.* **2008**, *71*, 308–319. [[CrossRef](#)] [[PubMed](#)]
13. Nord, J.; Larsson, G.; Kvassman, J.O.; Rosengren, A.M.; Nyman, P.O. dUTPase from the retrovirus equine infectious anemia virus: specificity, turnover and inhibition. *FEBS Lett.* **1997**, *414*, 271–274. [[PubMed](#)]
14. Larsson, G.; Nyman, P.O.; Kvassman, J.O. Kinetic characterization of dUTPase from Escherichia coli. *J. Biol. Chem.* **1996**, *271*, 24010–24016. [[CrossRef](#)] [[PubMed](#)]
15. Oliveros, M.; García-Escudero, R.; Alejo, A.; Viñuela, E.; Salas, M.L.; Salas, J. African swine fever virus dUTPase is a highly specific enzyme required for efficient replication in swine macrophages. *J. Virol.* **1999**, *73*, 8934–8943. [[PubMed](#)]
16. Nagy, G.N.; Leveles, I.; Vértessy, B.G. Preventive DNA repair by sanitizing the cellular (deoxy)nucleoside triphosphate pool. *FEBS J.* **2014**, *281*, 4207–4223. [[CrossRef](#)] [[PubMed](#)]
17. Sang, P.B.; Varshney, U. Biochemical Properties of MutT2 Proteins from Mycobacterium tuberculosis and M. smegmatis and Their Contrasting Antimutator Roles in Escherichia coli. *J. Bacteriol.* **2013**, *195*, 1552–1560. [[CrossRef](#)] [[PubMed](#)]
18. Varga, B.; Barabás, O.; Kovári, J.; Tóth, J.; Hunyadi-Gulyás, E.; Klement, E.; Medzihradzky, K.F.; Tölgyesi, F.; Fidy, J.; Vértessy, B.G. Active site closure facilitates juxtaposition of reactant atoms for initiation of catalysis by human dUTPase. *FEBS Lett.* **2007**, *581*, 4783–4788. [[CrossRef](#)]
19. Szabó, J.E.; Takács, E.; Merényi, G.; Vértessy, B.G.; Tóth, J. Trading in cooperativity for specificity to maintain uracil-free DNA. *Sci. Rep.* **2016**, *6*, 24219. [[CrossRef](#)]
20. Varga, B.; Barabás, O.; Takács, E.; Nagy, N.; Nagy, P.; Vértessy, B.G. Active site of mycobacterial dUTPase: structural characteristics and a built-in sensor. *Biochem. Biophys. Res. Commun.* **2008**, *373*, 8–13. [[CrossRef](#)]
21. Papp-Kádár, V.; Balázs, Z.; Vékey, K.; Ozohanics, O.; Vértessy, B.G. Mass spectrometry-based analysis of macromolecular complexes of Staphylococcus aureus uracil-DNA glycosylase and its inhibitor reveals specific variations due to naturally occurring mutations. *FEBS Open Bio* **2019**, *9*, 420–427. [[PubMed](#)]
22. Bartha-Vári, J.H.; Toşa, M.I.; Irimie, F.-D.; Weiser, D.; Boros, Z.; Vértessy, B.G.; Paizs, C.; Poppe, L. Immobilization of Phenylalanine Ammonia-Lyase on Single-Walled Carbon Nanotubes for Stereoselective Biotransformations in Batch and Continuous-Flow Modes. *ChemCatChem* **2015**, *7*, 1122–1128. [[CrossRef](#)] [[PubMed](#)]
23. Papp-Kádár, V.; Balázs, Z.; Nagy, G.N.; Juhász, T.; Liliom, K.; Vértessy, B.G. Functional analysis on a naturally occurring variant of the Staphylococcus Aureus uracil DNA Glycosylase inhibitor. *Period. Polytech. Chem. Eng.* **2018**, *62*, 51–56. [[CrossRef](#)]
24. Bata, Z.; Qian, R.; Roller, A.; Horak, J.; Bencze, L.C.; Paizs, C.; Hammerschmidt, F.; Vértessy, B.G.; Poppe, L. A Methylidene Group in the Phosphonic Acid Analogue of Phenylalanine Reverses the Enantiopreference of Binding to Phenylalanine Ammonia-Lyases. *Adv. Synth. Catal.* **2017**, *359*, 2109–2120. [[CrossRef](#)]
25. Takács, B.; Billington, N.; Gyimesi, M.; Kintses, B.; Málnási-Csizmadia, A.; Knight, P.J.; Kovács, M. Myosin complexed with ADP and blebbistatin reversibly adopts a conformation resembling the start point of the working stroke. *Proc. Natl. Acad. Sci. USA* **2010**, *107*, 6799–6804. [[CrossRef](#)]
26. Szabó, J.E.; Németh, V.; Papp-Kádár, V.; Nyíri, K.; Leveles, I.; Bendes, A.Á.; Zagyva, I.; Róna, G.; Pálincás, H.L.; Besztercei, B.; et al. Highly potent dUTPase inhibition by a bacterial repressor protein reveals a novel mechanism for gene expression control. *Nucleic Acids Res.* **2014**, *42*, 11912–11920. [[CrossRef](#)]
27. Li, H.; Robertson, A.D.; Jensen, J.H. Very fast empirical prediction and rationalization of protein pKa values. *Proteins Struct. Funct. Bioinforma.* **2005**, *61*, 704–721. [[CrossRef](#)]
28. Bas, D.C.; Rogers, D.M.; Jensen, J.H. Very fast prediction and rationalization of pKa values for protein-ligand complexes. *Proteins* **2008**, *73*, 765–783. [[CrossRef](#)]
29. Dolinsky, T.J.; Nielsen, J.E.; McCammon, J.A.; Baker, N.A. PDB2PQR: an automated pipeline for the setup of Poisson-Boltzmann electrostatics calculations. *Nucleic Acids Res.* **2004**, *32*, W665–W667. [[CrossRef](#)]
30. Cherrier, M.V.; Martin, L.; Cavazza, C.; Jacquamet, L.; Lemaire, D.; Gaillard, J.; Fontecilla-Camps, J.C. Crystallographic and spectroscopic evidence for high affinity binding of FeEDTA(H₂O)- to the periplasmic nickel transporter NikA. *J. Am. Chem. Soc.* **2005**, *127*, 10075–10082. [[CrossRef](#)]

31. Chemical Computing Group Inc. MOE (The Molecular Operating Environment) Version 2007.09, software available from Chemical Computing Group Inc., 1010 Sherbrooke Street West, Suite 910, Montreal, Canada H3A 2R7. 2007. Available online: <http://www.chemcomp.com> (accessed on 1 May 2013).
32. Halgren, T.A. Merck molecular force field. I. Basis, form, scope, parameterization, and performance of MMFF94. *J. Comput. Chem.* **1996**, *17*, 490–519. [[CrossRef](#)]
33. Halgren, T.A. Merck molecular force field. II. MMFF94 van der Waals and electrostatic parameters for intermolecular interactions. *J. Comput. Chem.* **1996**, *17*, 520–552. [[CrossRef](#)]
34. Halgren, T.A. Merck molecular force field. III. Molecular geometries and vibrational frequencies for MMFF94. *J. Comput. Chem.* **1996**, *17*, 553–586. [[CrossRef](#)]
35. Halgren, T.A.; Nachbar, R.B. Merck molecular force field. IV. conformational energies and geometries for MMFF94. *J. Comput. Chem.* **1996**, *17*, 587–615. [[CrossRef](#)]
36. Halgren, T.A. Merck molecular force field. V. Extension of MMFF94 using experimental data, additional computational data, and empirical rules. *J. Comput. Chem.* **1996**, *17*, 616–641. [[CrossRef](#)]
37. Gasteiger, J.; Marsili, M. Iterative partial equalization of orbital electronegativity—a rapid access to atomic charges. *Tetrahedron* **1980**, *36*, 3219–3228. [[CrossRef](#)]
38. Morris, G.M.; Huey, R.; Lindstrom, W.; Sanner, M.F.; Belew, R.K.;Goodsell, D.S.; Olson, A.J. AutoDock4 and AutoDockTools4: Automated docking with selective receptor flexibility. *J. Comput. Chem.* **2009**, *30*, 2785–2791. [[CrossRef](#)] [[PubMed](#)]
39. Morris, G.M.;Goodsell, D.S.; Halliday, R.S.; Huey, R.; Hart, W.E.; Belew, R.K.; Olson, A.J. Automated docking using a Lamarckian genetic algorithm and an empirical binding free energy function. *J. Comput. Chem.* **1998**, *19*, 1639–1662. [[CrossRef](#)]
40. Hetényi, C.; van der Spoel, D. Efficient docking of peptides to proteins without prior knowledge of the binding site. *Protein Sci.* **2002**, *11*, 1729–1737. [[CrossRef](#)]
41. Hetényi, C.; van der Spoel, D. Blind docking of drug-sized compounds to proteins with up to a thousand residues. *FEBS Lett.* **2006**, *580*, 1447–1450. [[CrossRef](#)]
42. Clark, A.M.; Labute, P. 2D depiction of protein-ligand complexes. *J. Chem. Inf. Model.* **2007**, *47*, 1933–1944. [[CrossRef](#)] [[PubMed](#)]
43. Róna, G.; Marfori, M.; Borsos, M.; Scheer, I.; Takács, E.; Tóth, J.; Babos, F.; Magyar, A.; Erdei, A.; Bozóky, Z.; et al. Phosphorylation adjacent to the nuclear localization signal of human dUTPase abolishes nuclear import: structural and mechanistic insights. *Acta Crystallogr. D. Biol. Crystallogr.* **2013**, *69*, 2495–2505. [[CrossRef](#)] [[PubMed](#)]
44. Keller, S.; Vargas, C.; Zhao, H.; Piszczek, G.; Brautigam, C.A.; Schuck, P. High-precision isothermal titration calorimetry with automated peak-shape analysis. *Anal. Chem.* **2012**, *84*, 5066–5073. [[CrossRef](#)] [[PubMed](#)]
45. Zhao, H.; Piszczek, G.; Schuck, P. SEDPHAT—A platform for global ITC analysis and global multi-method analysis of molecular interactions. *Methods* **2015**, *76*, 137–148. [[CrossRef](#)] [[PubMed](#)]
46. Brautigam, C.A.; Zhao, H.; Vargas, C.; Keller, S.; Schuck, P. Integration and global analysis of isothermal titration calorimetry data for studying macromolecular interactions. *Nat. Protoc.* **2016**, *11*, 882–894. [[CrossRef](#)] [[PubMed](#)]
47. Brautigam, C.A. Calculations and Publication-Quality Illustrations for Analytical Ultracentrifugation Data. *Methods Enzymol.* **2015**, *562*, 109–133. [[PubMed](#)]
48. Humphrey, W.; Dalke, A.; Schulten, K. VMD: visual molecular dynamics. *J. Mol. Graph.* **1996**, *14*, 33–38. [[CrossRef](#)]
49. Schrödinger LLC. The PyMOL Molecular Graphics System, Version 1.2r3pre. Available online: <http://www.schrodinger.com/pymol> (accessed on 19 October 2018).
50. Zhang, W.; Truttman, A.C.; Lüthi, D.; McGuigan, J.A. Apparent Mg²⁺-adenosine 5-triphosphate dissociation constant measured with Mg²⁺ macroelectrodes under conditions pertinent to ³¹P NMR ionized magnesium determinations. *Anal. Biochem.* **1997**, *251*, 246–250. [[CrossRef](#)]
51. Tóth, J.; Varga, B.; Kovács, M.; Málnási-Csizmadia, A.; Vértessy, B.G. Kinetic Mechanism of Human dUTPase, an Essential Nucleotide Pyrophosphatase Enzyme. *J. Biol. Chem.* **2007**, *282*, 33572–33582. [[CrossRef](#)]
52. Lopata, A.; Jambrina, P.G.; Sharma, P.K.; Brooks, B.R.; Toth, J.; Vértessy, B.G.; Rosta, E. Mutations Decouple Proton Transfer from Phosphate Cleavage in the dUTPase Catalytic Reaction. *ACS Catal.* **2015**, *5*, 3225–3237. [[CrossRef](#)]

53. Sanner, M.F.; Olson, A.J.; Spehner, J.C. Reduced surface: An efficient way to compute molecular surfaces. *Biopolymers* **1996**, *38*, 305–320. [[CrossRef](#)]
54. Barabás, O.; Pongrácz, V.; Kovári, J.; Wilmanns, M.; Vértessy, B.G. Structural insights into the catalytic mechanism of phosphate ester hydrolysis by dUTPase. *J. Biol. Chem.* **2004**, *279*, 42907–42915. [[CrossRef](#)] [[PubMed](#)]
55. Barabás, O.; Németh, V.; Bodor, A.; Perczel, A.; Rosta, E.; Kele, Z.; Zagyva, I.; Szabadka, Z.; Grolmusz, V.I.; Wilmanns, M.; et al. Catalytic mechanism of α -phosphate attack in dUTPase is revealed by X-ray crystallographic snapshots of distinct intermediates, 31P-NMR spectroscopy and reaction path modelling. *Nucleic Acids Res.* **2013**, *41*, 10542–10555. [[CrossRef](#)] [[PubMed](#)]
56. Hirmondo, R.; Lopata, A.; Suranyi, E.V.; Vértessy, B.G.; Toth, J. Differential control of dNTP biosynthesis and genome integrity maintenance by the dUTPase superfamily enzymes. *Sci. Rep.* **2017**, *7*, 6043. [[CrossRef](#)] [[PubMed](#)]
57. Pecsí, I.; Szabo, J.E.; Adams, S.D.; Simon, I.; Sellers, J.R.; Vértessy, B.G.; Toth, J. Nucleotide pyrophosphatase employs a P-loop-like motif to enhance catalytic power and NDP/NTP discrimination. *Proc. Natl. Acad. Sci.* **2011**, *108*, 14437–14442. [[CrossRef](#)] [[PubMed](#)]
58. O'Brien, L.C.; Root, H.B.; Wei, C.-C.; Jensen, D.; Shabestary, N.; De Meo, C.; Eder, D.J. M2+ •EDTA Binding Affinities: A Modern Experiment in Thermodynamics for the Physical Chemistry Laboratory. *J. Chem. Educ.* **2015**, *92*, 1547–1551. [[CrossRef](#)]
59. Brandis, J.W.; Edwards, S.G.; Johnson, K.A. Slow rate of phosphodiester bond formation accounts for the strong bias that Taq DNA polymerase shows against 2',3'-dideoxynucleotide terminators. *Biochemistry* **1996**, *35*, 2189–2200. [[CrossRef](#)] [[PubMed](#)]
60. Maki, H.; Sekiguchi, M. MutT protein specifically hydrolyses a potent mutagenic substrate for DNA synthesis. *Lett. Nat.* **1992**, *355*, 273–275. [[CrossRef](#)]
61. Carvajal, N.; Orellana, M.S.; Bórquez, J.; Uribe, E.; López, V.; Salas, M. Non-chelating inhibition of the H101N variant of human liver arginase by EDTA. *J. Inorg. Biochem.* **2004**, *98*, 1465–1469. [[CrossRef](#)]
62. Shah, M.; Grover, T.; Barr, D.; Aust, S. On the mechanism of inhibition of the veratryl alcohol oxidase activity of lignin peroxidase H2 by EDTA. *J. Biol. Chem.* **1992**, *267*, 21564–21569.
63. Banerjee, R.K. EDTA inhibits peroxidase-catalyzed iodide oxidation through interaction at the iodide binding site. *Biochim. Biophys. Acta - Gen. Subj.* **1989**, *992*, 393–396. [[CrossRef](#)]
64. Bhattacharyya, D.K.; Adak, S.; Bandyopadhyay, U.; Banerjee, R.K. Mechanism of inhibition of horseradish peroxidase-catalysed iodide oxidation by EDTA. *Biochem. J.* **1994**, *298* (Pt 2), 281–288. [[CrossRef](#)]
65. Ding, Y.; Williams, R.M.; Sherman, D.H. Molecular analysis of a 4-dimethylallyltryptophan synthase from *Malbranchea aurantiaca*. *J. Biol. Chem.* **2008**, *283*, 16068–16076. [[CrossRef](#)]
66. Kondoh, G.; Tojo, H.; Nakatani, Y.; Komazawa, N.; Murata, C.; Yamagata, K.; Maeda, Y.; Kinoshita, T.; Okabe, M.; Taguchi, R.; et al. Angiotensin-converting enzyme is a GPI-anchored protein releasing factor crucial for fertilization. *Nat. Med.* **2005**, *11*, 160–166. [[CrossRef](#)] [[PubMed](#)]
67. Hast, M.A.; Fletcher, S.; Cummings, C.G.; Pusateri, E.E.; Blaskovich, M.A.; Rivas, K.; Gelb, M.H.; Van Voorhis, W.C.; Sebtí, S.M.; Hamilton, A.D.; et al. Structural basis for binding and selectivity of antimalarial and anticancer ethylenediamine inhibitors to protein farnesyltransferase. *Chem. Biol.* **2009**, *16*, 181–192. [[CrossRef](#)] [[PubMed](#)]
68. Fletcher, S.; Keaney, E.P.; Cummings, C.G.; Blaskovich, M.A.; Hast, M.A.; Glenn, M.P.; Chang, S.-Y.; Bucher, C.J.; Floyd, R.J.; Katt, W.P.; et al. Structure-based design and synthesis of potent, ethylenediamine-based, mammalian farnesyltransferase inhibitors as anticancer agents. *J. Med. Chem.* **2010**, *53*, 6867–6888. [[CrossRef](#)] [[PubMed](#)]
69. Delarue, M.; Poch, O.; Tordo, N.; Moras, D.; Argos, P. An attempt to unify the structure of polymerases. *Protein Eng.* **1990**, *3*, 461–467. [[CrossRef](#)] [[PubMed](#)]
70. Kropp, H.M.; Diederichs, K.; Marx, A. The Structure of an Archaeal B-Family DNA Polymerase in Complex with a Chemically Modified Nucleotide. *Angew. Chem. Int. Ed. Engl.* **2019**, *58*, 5457–5461. [[CrossRef](#)] [[PubMed](#)]
71. Nakamura, T.; Meshitsuka, S.; Kitagawa, S.; Abe, N.; Yamada, J.; Ishino, T.; Nakano, H.; Tsuzuki, T.; Doi, T.; Kobayashi, Y.; et al. Structural and dynamic features of the MutT protein in the recognition of nucleotides with the mutagenic 8-oxoguanine base. *J. Biol. Chem.* **2010**, *285*, 444–452. [[CrossRef](#)]

72. Yang, Y.; Gourinath, S.; Kovács, M.; Nyitray, L.; Reutzel, R.; Himmel, D.M.; O’Neill-Hennessey, E.; Reshetnikova, L.; Szent-Györgyi, A.G.; Brown, J.H.; et al. Rigor-like structures from muscle myosins reveal key mechanical elements in the transduction pathways of this allosteric motor. *Structure* **2007**, *15*, 553–564. [[CrossRef](#)]
73. Moeschler, H.J.; Schaer, J.J.; Cox, J.A. A thermodynamic analysis of the binding of calcium and magnesium ions to parvalbumin. *Eur. J. Biochem.* **1980**, *111*, 73–78. [[CrossRef](#)] [[PubMed](#)]
74. Lopata, A.; Leveles, I.; Bendes, Á.Á.; Viskolcz, B.; Vértessy, B.G.; Jójárt, B.; Tóth, J. A Hidden Active Site in the Potential Drug Target Mycobacterium tuberculosis dUTPase Is Accessible through Small Amplitude Protein Conformational Changes. *J. Biol. Chem.* **2016**, *291*, 26320–26331. [[CrossRef](#)] [[PubMed](#)]
75. Mónico, A.; Martínez-Sendra, E.; Cañada, F.J.; Zorrilla, S.; Pérez-Sala, D. Drawbacks of Dialysis Procedures for Removal of EDTA. *PLoS ONE* **2017**, *12*, e0169843. [[CrossRef](#)] [[PubMed](#)]
76. Sharpe, J.C.; London, E. Inadvertent Concentrating of EDTA by Ion Exchange Chromatography: Avoiding Artifacts That Can Interfere with Protein Purification. *Anal. Biochem.* **1997**, *250*, 124–125. [[CrossRef](#)]
77. Chumanov, R.S.; Burgess, R.R. Artifact-inducing enrichment of ethylenediaminetetraacetic acid and ethyleneglycoltetraacetic acid on anion exchange resins. *Anal. Biochem.* **2011**, *412*, 34–39. [[CrossRef](#)]



© 2019 by the authors. Licensee MDPI, Basel, Switzerland. This article is an open access article distributed under the terms and conditions of the Creative Commons Attribution (CC BY) license (<http://creativecommons.org/licenses/by/4.0/>).